Int. J. Electrochem. Sci., 8 **(2013)** 2536 - 2550

International Journal of
ELECTROCHEMICAL
SCIENCE
www.electrochemsci.org

Corrosion Evolution of Scaled Rebar in Concrete under Dry/wet Cyclic Condition in 3.5% NaCl Solution

J. Wei, J. H. Dong[*]*, W. Ke*

State Key Laboratory of Corrosion and Protection, Institute of Metal Research, Chinese Academy of Sciences, 62 Wencui Road, Shenyang 110016, China
[*]E-mail: jhdong@imr.ac.cn.

Received: 20 November 2012 / *Accepted:* 11 December 2012 / *Published:* 1 February 2013

The evolution of water-cooled scaled rebar corroded in concrete under alternate dry/wet corrosion acceleration condition with 3.5% NaCl solution was studied by EIS, potential monitoring, SEM and XRD techniques. The results show that the corrosion evolution of rebar undergoes uniform corrosion in three stages. The initial stage is described as the charge transfer process, which starts from the concrete curing period due to the porous scale of water-cooled rebar. The second stage is described as the corrosion acceleration process which attributes to the gradually increase of scale pores caused by Cl^- penetration. The third stage is described as the steady corrosion process due to the diffusion limitation through a thick rust layer.

Keywords: Scaled rebar, Corrosion evolution, EIS, Concrete, Chloride

1. INTRODUCTION

Chloride-induced corrosion of rebar in reinforced concrete is one of the major causes of deterioration of reinforced concrete (RC) structures [1-3]. Specifically, in the splash zone of marine environment, the alternating dry and wet corrosive environment accelerates the corrosion processes of rebar in concrete, which leads to the durability of marine structures, such as cross sea bridge, seabed tunnel, oil production platforms and offshore breakwater, decrease significantly [4-6]. Therefore, evaluating the corrosion rate of rebar in concrete and understanding its corrosion processes under alternating dry and wet conditions play important roles in predicting the service life of RC structures and establishing the reasonable protection techniques.

At present, the researches on corrosion evolution of rebar in concrete mainly focus on bare rebar. It is well known that in the high alkaline concrete environment that free of aggressive ions, such as Cl^-, SO_4^{2-} and CO_3^{2-} etc, a layer of compact passive film forms on the surface of bare rebar which

can protect the steel from corrosion [7-8]. However, as this passive film is only a few tens of Angstroms [9-10], it may be destroyed at local weak regions in the film if there are aggressive ions in concrete and the content of the aggressive ions reach its threshold content [11-12]. Studies on corrosion evolution of bare rebar in concrete show that the corrosion type of bare rebar in chloride contaminated concrete gradually transform from the initial pitting corrosion to the uniform corrosion, and the corrosion rate firstly increases and then decreases [13-15].

In spite of corrosion of bare rebar in concrete has been extensively studied, the scaled rebar is widely applied in actual RC structures rather than bare rebar to simplify the descaling procedure and save cost [16]. At present, limited researches on corrosion of scaled rebar in concrete all adopt simulated concrete solution as the environment system. Xing reports that like the passivation of bare rebar in high alkaline environment, the scaled rebar can also maintain in passive state. Furthermore, the scaled rebar shows better corrosion resistance than the bare rebar against Cl^- [17]. However, Ghods reported that the scaled rebar is easier to depassivation than bare rebar in chloride contaminated concrete [18-19]. It is because crevice corrosion happens to the scaled rebar. The disagreement may be attributed to the different oxide scales on the rebar surface in the above two researches. For scaled rebar, the oxide scale forms during the cooling process after finish rolling during the production of the hot-rolled rebar. And the compositions and structure of the scale can be influenced by different cooling processes [20]. According to the different cooling ways, the scaled rebar can be divided into the air-cooled rebar and water-cooled rebar. Our previous studies show that the compositions of both rebar scales consist of FeO, Fe_3O_4 and Fe_2O_3. The thickness of the scale is about 20 μm. However, the structure and compactness of the scale differs significantly. The scale on water-cooled rebar is loose and porous, and it shows weak bonding performance to the substrate. Therefore, it is easy for the corrosive medium to penetrate and cause corrosion. However, the compactness and the bonding performance of scale on air-cooled rebar are superior to those of water-cooled rebar. Therefore, the corrosion resistance of air-cooled rebar in the atmosphere and concrete are better than those of water-cooled rebar [20-22].

Obviously, the surface state of oxide scale will influence the corrosion evolution processes of rebar in concrete with chloride under alternating wet and dry corrosive condition, and it will finally affect the durability of RC structures. The current work focused on studying the corrosion evolution of the water-cooled rebar in concrete under alternate dry/wet accelerated corrosion condition with NaCl solution and evaluating the corrosion resistance of water-cooled rebar.

2. EXPERIMENTAL PART

2.1 Material and Procedures

2.1.1 Rebar sample preparation

The commercial 20SiMn hot-rolled rebar was used in the experiment, with chemical composition (wt.%): C 0.17~0.25, Si 0.40~0.80, Mn 1.20~1.60, P 0.050, S 0.050. The rebar samples

were machined into cylinders (Φ10mm×60mm) and the surfaces were polished using 1200# sand paper. The preparation of the water-cooled rebar simulates the on-line heating and cooling procedures to obtain the same scale. The machined samples were heated to 1000°C for 10 minutes in the pipe furnace under an anti-oxidizing flux protection, followed by cooling in water for 1 s. Then, the samples were cooled in air to the room temperature.

2.1.2 Concrete sample preparation

RC samples (80 mm in diameter and 80 mm in height) were cast according to standard experimental procedures using ordinary Portland cement 42.5 (with a water/cement ratio of 0.5 and cement/sand ratio of 1/3). The schematic diagram of the electrode system is shown in Figure 1, and all the length units are in millimeter. A three-electrode cell was used in this experiment. The working electrode (WE) was the machined rebar sample. Both ends of the rebar were coated with dense epoxy, leaving an exposed length of 40 mm. The rebar was positioned at the center of the concrete sample with a cover thickness of 35 mm. The reference electrode (RE) was $Cu/CuSO_4$ saturated electrode (CSE) which was positioned 5 mm near the working electrode to reduce the IR drop between WE and RE. In order to distribute the electrical signal uniformly, a 60 mm height annular graphite electrode was used as the counter electrode (CE), which was positioned in the concrete with the cover thickness of 11 mm. After demoulding at one day after casting, the concrete samples were cured in a standard curing chamber at 20±1°C and ≥95% RH for 28 days. In order to avoid the non-uniform penetration of solution, both ends of the concrete samples were coated with epoxy resin leaving 40 mm height profile exposed.

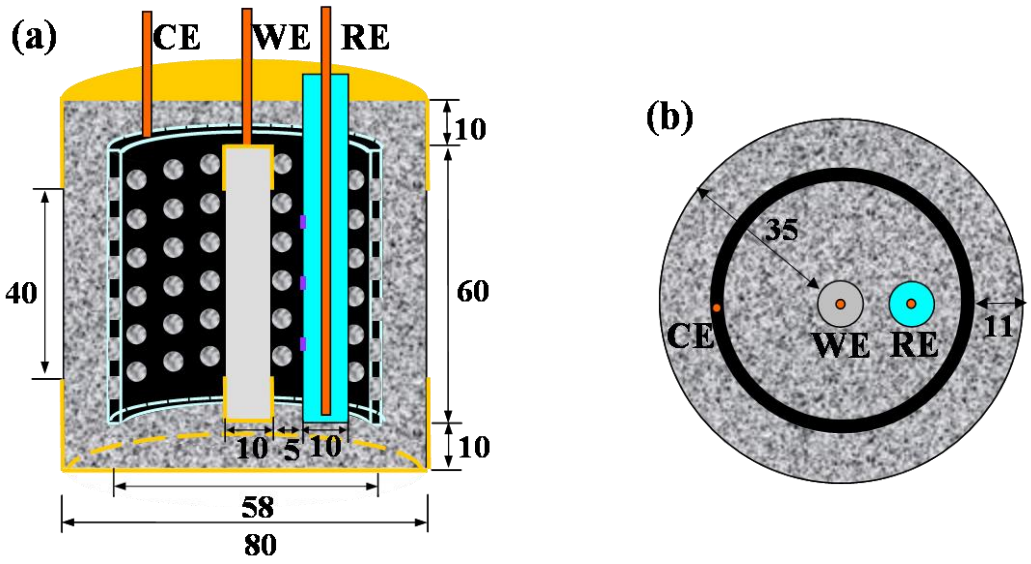

Figure 1. Schematic diagram of the electrode system for reinforced mortar samples. (a) side sectional view, (b) top sectional view.

2.2 Dry/wet cyclic accelerated corrosion tests

Before the dry/wet cyclic tests, the samples were immersed in de-ionized water for 1 day which was referred to as cycle 0. Then, 14 cycles of severe dry/wet cyclic corrosion tests were carried out to accelerate the corrosion of rebar in mortar. During each cycle, the samples are dried at 80°C for 4 days in a drying cabinet and then immersed in 3.5% sodium chloride solution (25°C) for 1 day. Both the drying and immersing processes can make the mortar samples reach a constant weight.

2.3 Electrochemical measurement

After each dry/wet cycle, E_{corr} and EIS were measured when the mortar samples were immersed in 3.5% sodium chloride solution, using a PAR 273A potentiostat and a PAR 5210E lock-in amplifier. EIS measurements were carried out at the open-circuit potential with a 10 mV perturbation from 100 kHz to 10 mHz. All the measurements were carried out at room temperature (25°C). The EIS results were fitted by ZSimpWin software based on the equivalent circuit models.

2.4 SEM Analysis

A HITACHI S3400N scanning electronic microscope was used to observe the surface morphologies of oxide scale on the rebar before corrosion tests, the cross section morphology of the corrosion products after 14 dry/wet cycles' corrosion test and the corrosion morphology of the rebar after removing the rust.

2.5 XRD Analysis

To analyze the compositions of the corrosion product, XRD experiment was carried out using a Rigaku-D/max 2000 diffractometer by employing a Cu target under 50kV×250mA. The scan rate was 2°/min. The powder sample used for XRD analysis was prepared by grinding the corrosion products scraped from the rebar surface.

3. RESULTS

3.1 Evolution of E_{corr}

Figure 2 shows the evolution of E_{corr} with dry/wet cycles for the rebar, which was measured after each dry/wet cycle when the mortar was immersed in sodium chloride solution. The ASTM C876 standard [23] has determined three E_{corr} levels to identify the corrosion probability of rebar in concrete. That is, when E_{corr} > -0.20V (vs. CSE), the corrosion probability of rebar in concrete is less than 10%; when E_{corr} < -0.35V (vs. CSE), the corrosion probability of rebar in concrete is more than 90%; and when it locates between -0.35V (vs. CSE) and -0.20V (vs. CSE), the probability is uncertain. It is

shown that E_{corr} of rebar locates in the region in which the corrosion probability is larger than 90% during all the dry/wet alternated cycles, which indicates that unlike the passivation of bare rebar in high alkaline concrete, the water-cooled rebar has been corroded since the initial curing period. Furthermore, E_{corr} decreases from cycle 0 to 4, which implies that the rebar is easier to corrode with increasing the cycles.

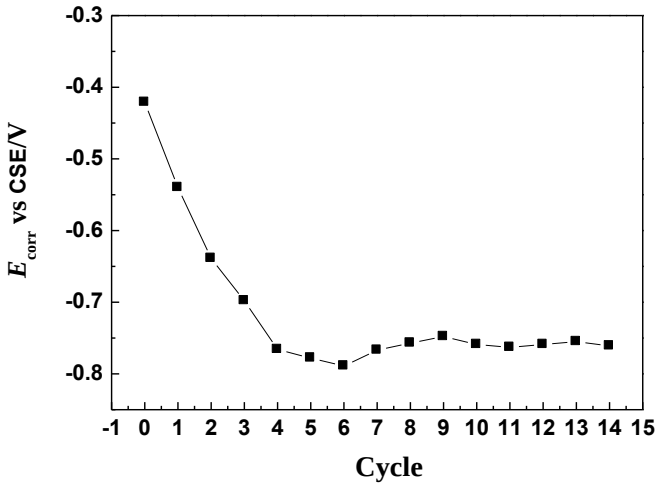

Figure 2. Evolution of E_{corr} with dry/wet cycles.

3.2 Evolution of the EIS spectra

Figure 3 shows the impedance Bode plots of rebar in mortar after each cycle of the alternate dry/wet corrosion test. For the Bode |Z| plots, the high frequency impedance corresponds to the solution resistance (R_s). The low frequency impedance corresponds to the total impedance, which equals to the sum of the solution resistance (R_s), film resistance (R_f), rust resistance (R_r) and the charge transfer resistance (R_{ct}).

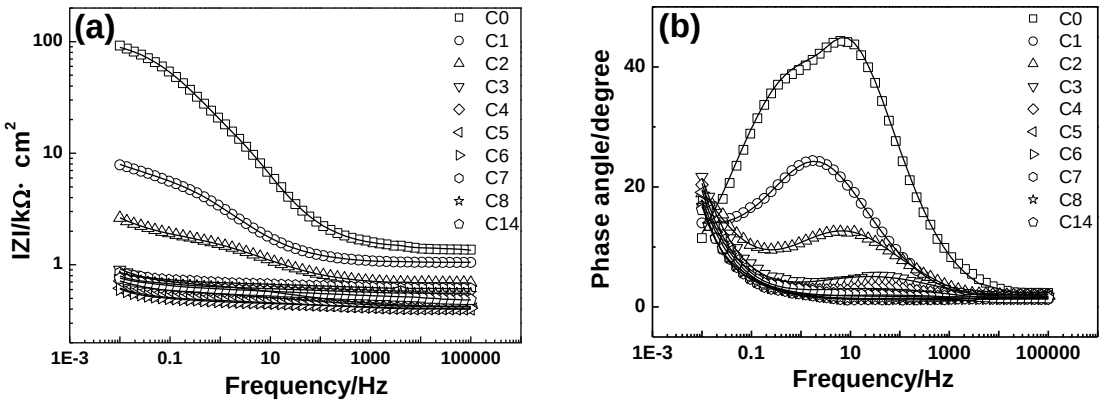

Figure 3. Bode plots of water-cooled rebar in mortar for cycle1~cycle8 and cycle14. Solid lines represent the fitting results. (a) Bode |Z| plot, (b) Bode phase plot.

Figure 3(a) shows that the total impedance decreases sharply with increasing the cycles, indicating an increase of the corrosion rate. After cycle 5, the change in the low frequency impedance is very limited. At the same time, as shown in the Bode phase plot in Figure 3(b), the peak value of the phase angle also decreases with increasing cycles, which indicates a decay of the capacitive impedance of the surface film. As the capacitance of the surface film represents the penetrability of the film, this decay of capacitive impedance means that the penetrability of the film increases with increasing the immersion time and more ions can reach the matrix through the film to erode the steel [24, 25]. After cycle 1, the phase angle occurs a diffusion tail at low frequency region, which indicates that the mass transfer behavior occurs on the rebar/concrete interface [26]. After cycle 5, the peak value of phase angle in the middle frequency decreases to a minimum value. The difference in the Bode phase plot after cycle 5 becomes negligible.

3.3 Transformation of the concrete/rebar interface

The changes in the impedance spectra indicate that the corrosion of rebar undergoes complicated evolution processes and exhibits different corrosion dynamic characteristics during dry/wet cycles [27]. These corrosion evolutions correspond to changes of the interface state between rebar and concrete.

The initial surface state affects the corrosion type and the corrosion process significantly. Figure 4 shows the initial surface morphology of the oxide scale on rebar. It is obvious that many pores distribute in the whole oxide scale. As the aggressive mediums such as water, oxygen and chloride ions may penetrate through the pores in the scale reaching the rebar surface, the scale is thus unfavorable against corrosion.

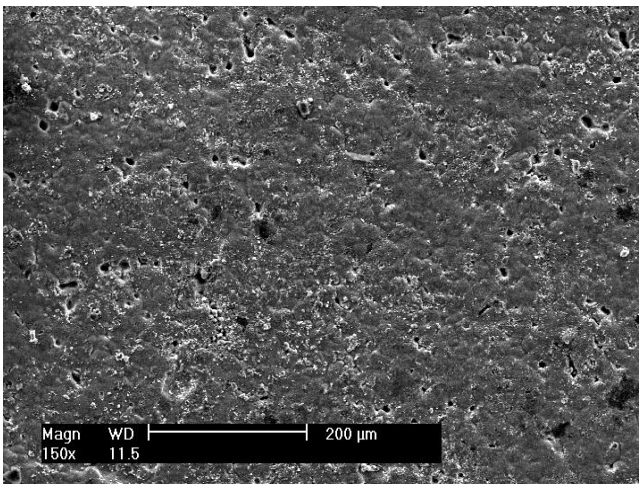

Figure 4. Surface morphology of the scale on water-cooled rebar.

Figure 5 shows the surface morphology of the rebar after curing. It is evident that many small rust spots uniformly distribute on the rebar surface which indicates that uniform corrosion occurs on

rebar during the curing period. The rust forms at the scale/ rebar interface and grows out of the scale to damage the scale.

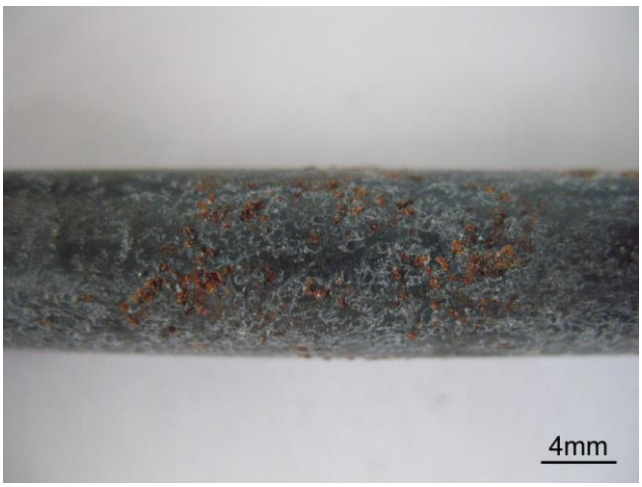

Figure 5. Corrosion morphology of the rebar after curing.

Figure 6. Corrosion morphology of the rebar after 14 cycles corrosion.

After 14 dry/wet cycles, the corrosion morphology is shown in Figure 6. Thick rust layer forms on rebar surface. When took the rebar out of the concrete, most of the outer rust had pulled off with the concrete, and only on some small area the initial scale was remained. The cross section morphology of the corrosion product of the rebar is shown in Figure 7. The rust thickness is about 250 μm. The large volume of rust induces some cracks and holes in the rust. Moreover, the scale looks porous and damaged. The surface morphology of the rebar after removing the rust is shown in Figure 8. The surface of the rebar looks flat, and small corrosion pits distribute uniformly on the whole surface, also indicative of uniform corrosion.

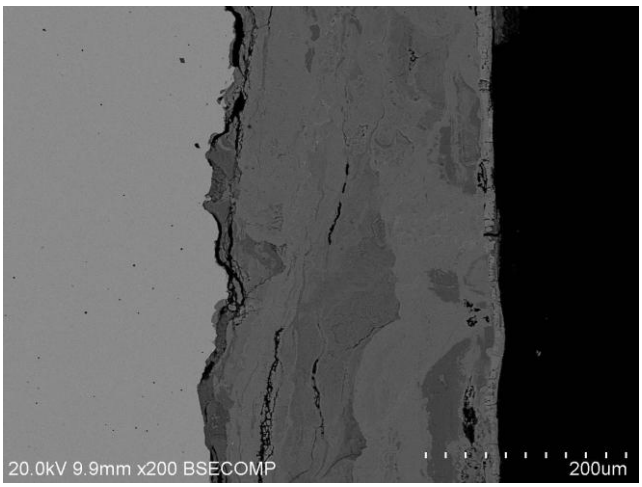

Figure 7. Cross section morphology of the corroded rebar.

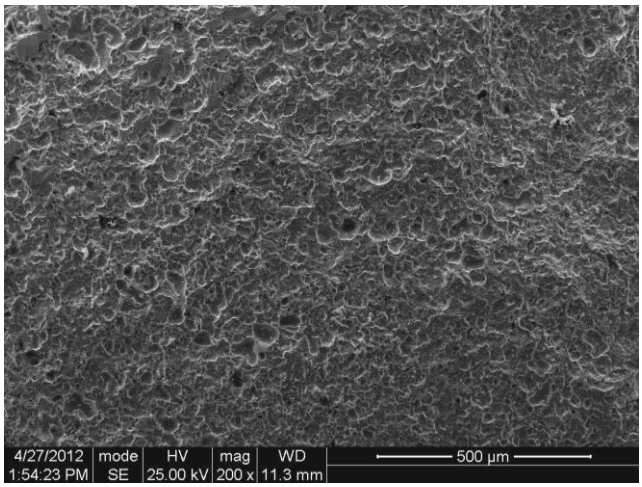

Figure 8. Corrosion morphology of the rebar substrate after removing the scale.

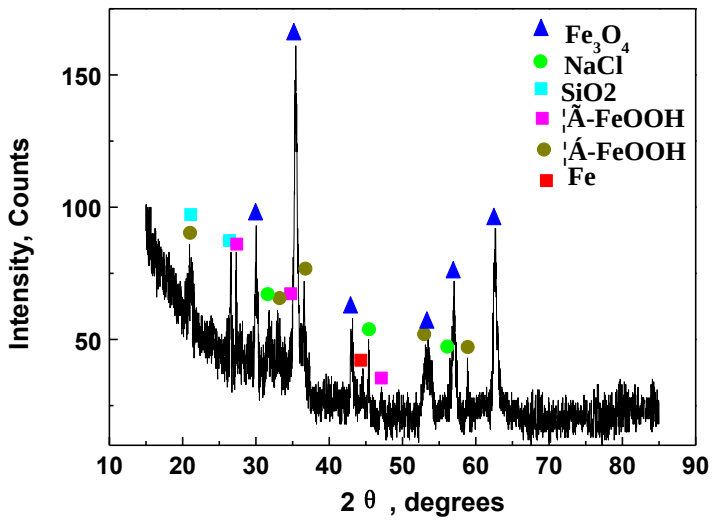

Figure 9. XRD patterns of the corrosion product formed on water-cooled rebar.

Figure 9 shows XRD patterns of corrosion product formed on rebar. The phases of Fe, NaCl and SiO_2 examined in the XRD pattern are introduced from rebar substrate and the mortar during the sample preparation. The corrosion product of rebar is composed of γ-FeOOH, Fe_3O_4 and α-FeOOH.

3.4 Analyses of the corrosion evolution processes

According to the characteristics of the electrochemical results and the surface states of the rebar before and after corrosion, the corrosion evolution processes were analyzed by constructing the interface structure models and the equivalent circuit (EC) models, as shown in Figure 10.

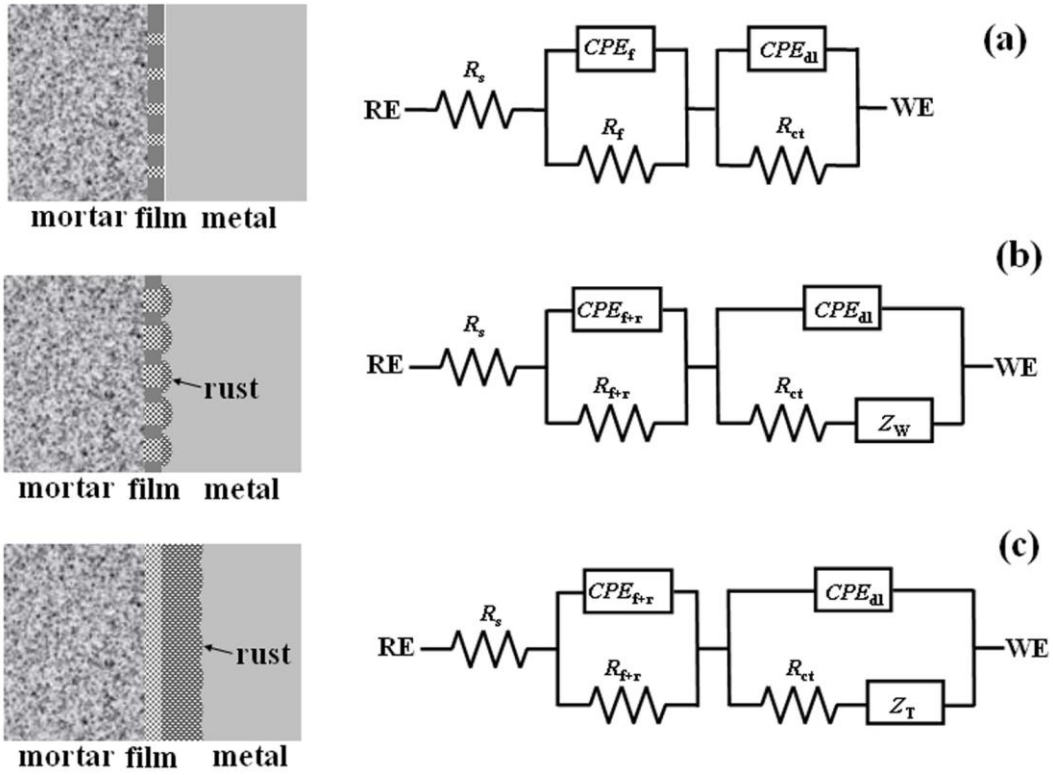

Figure 10. Interface structure models and the EC models for water-cooled rebar. (a) stage Ⅰ, (b) stage Ⅱ, (c) stage Ⅲ.

The corrosion evolution undergoes three stages for the rebar. In the curing period of cycle 0, the E_{corr} locates in the high corrosion probability region, and the total impedance is only about 100 $k\Omega \cdot cm^2$ (as shown in Figure 10(a)). That indicates that the rebar is in active corrosion state. During the curing period, the concrete samples maintain in the constant temperature and humidity condition of 20°C and 95% RH. Water and oxygen can transfer to the concrete/rebar interface from the pores in concrete. Furthermore, these mediums can also reach the rebar substrate through the pores in the oxide scale. As the potential of rebar substrate and oxide scale is different, the corrosion galvanic cell forms when the oxide scale acts as cathode and the rebar substrate acts as anode. Therefore, galvanic

corrosion occurs on rebar. As the porous scale benefits the transportation of reactants and products to and from the rebar surface in cycle 0, the diffusion process can satisfy the need of the electrode reactions. Thus, stage Ⅰ (cycle 0) corresponds to the state that the rebar is in active state and the charge transfer is the rate determining step of corrosion process. In the EC model, R_s stands for the solution resistance of concrete pores between RE and WE, R_f the resistance of the surface film, CPE_f the constant phase element of the surface film, R_{ct} the charge transfer resistance, and CPE_{dl} the constant phase element of the electric double layer. In the concrete system, the film capacitance and electric double layer capacitance usually deviate from pure capacitance due to the dispersion effect, and the constant phase element (CPE) is used instead of pure capacitance [28-30].

As corrosion proceeds, the penetration of Cl^- and the volume expansion caused by corrosion products enlarges the broken area of the oxide scale. Therefore, both the diffusion process and charge transfer process are accelerated which leads to the obvious corrosion acceleration of the rebar. Furthermore, with the gradually thickening of corrosion products on the anode regions of rebar, the transportation of reactants and products become slower than the charge transfer. Therefore, the diffusion process instead of the charge transfer process dominates the corrosion rate. According to the EIS spectra, the phase angle plots present a diffusion tail at the low frequency region after cycle 1, which also indicates that the mass transfer behavior occurs on the rebar/concrete interface. Stage Ⅱ (cycle 1~4) corresponds to the state that the broken area on the scale is enlarged and a thin rust layer forms on anode regions of rebar substrate. The rate of charge transfer increases faster than the diffusion rate, and the diffusion process becomes the slow step of the electrode process as shown in Figure 10 (b). In the EC model, R_{f+r} stands for the total resistance of the passive film and the rust, CPE_{f+r} the total constant phase element of the passive film and the rust, and Z_W [31] the Warburg resistance of the semi-infinite diffusion process.

With further increasing the dry/wet cycles, a thick rust layer forms on the rebar surface which may block the diffusion of reactants and products. Stage Ⅲ (cycle 5~14) corresponds to the state that the electrode process is controlled by the diffusion process through a thick rust layer, as shown in Figure 10 (c). In the EC model, R_r stands for the resistance of rust layer, CPE_r the capacitance of rust layer, Z_T barrier layer diffusion resistance [32].

3.5 Fitting results of EIS

The fitting curves are presented in Figure 3 as solid lines and the fitting parameters are listed in Table 1. The resistances of R_f and R_{f+r} are expressed as R_1, and the constant phase element of CPE_f and CPE_{f+r} are expressed as CPE_1.

R_s decreases in the earlier cycles, and it then increases in the subsequent cycles. It correlates to the accumulation of salt transmitted to the mortar. The decrease of R_s is caused by the continuous penetration and deposition of NaCl into the mortar during the dry/wet cycles. The penetrated NaCl saturates the pore solution at cycle 3, and R_s changes a little from cycle 3 to 6. Thereafter, some of the corrosion products fill the pores of the mortar, resisting to the penetration of ions and resulting in an increase of R_s.

Table 1. Fitting results of EIS data of water-cooled rebar

cycle	R_s ($k\Omega \cdot cm^2$)	CPE_1-$Y_0 \times 10^4$ ($\Omega^{-1} \cdot cm^{-2} \cdot s^{-n1}$)	n_1	R_1 ($k\Omega \cdot cm^2$)	CPE_{dl}-$Y_0 \times 10^4$ ($\Omega^{-1} \cdot cm^{-2} \cdot s^{-ndl}$)	n_{dl}	R_{ct} ($k\Omega \cdot cm^2$)	W-$Y_0 \times 10^4$ ($\Omega^{-1} \cdot cm^{-2} \cdot s^{-0.5}$)	T-$Y_0 \times 10^4$ ($\Omega^{-1} \cdot cm^{-2} \cdot s^{-0.5}$)	T-B ($s^{-0.5}$)	$\chi^2 \times 10^4$
0	1.42	0.20	0.90	3.29	0.18	0.61	103.30				3.33
1	1.03	1.45	0.65	2.69	3.48	0.45	5.91	19.11			0.17
2	0.67	1.91	0.50	1.25	54.84	0.77	1.22	25.13			0.22
3	0.41	5.40	0.41	0.29	187.0	0.78	0.33	27.87			0.56
4	0.40	10.93	0.33	0.20	279.4	0.84	0.11	28.63			0.16
5	0.38	16.74	0.28	0.18	326.6	0.78	0.08		34.97	5.45	0.16
6	0.36	27.38	0.17	0.16	343.3	0.74	0.07		28.09	5.63	0.16
7	0.59	24.07	0.24	0.17	272.0	0.83	0.07		49.28	4.59	0.30
8	0.54	20.80	0.27	0.14	256.5	0.77	0.07		45.45	4.40	0.27
14	0.48	16.04	0.24	0.18	233.6	0.70	0.07		40.09	3.80	0.74

According to the evolution of R_1 with dry/wet cycles, the corrosion resistance of the scale can be analyzed. R_1 equals to 3.29 $k\Omega \cdot cm^2$ at cycle 0 and decreased sharply during stage Ⅱ. It indicates that the resistant ability of the scale against the aggressive ions decreases and more aggressive ions can transfer to the rebar substrate to corrode the rebar. From stage Ⅲ, R_1 changes slightly with the dry/wet cycles, which corresponds to the combined action of continuous decrease of R_f and increase of R_r with the dry/wet cycles.

Similarly to R_1, R_{ct} also decreased sharply during stage Ⅱ and remained fairly constant in stage Ⅲ. The decrease of R_{ct} in stage Ⅱ indicates the acceleration of the charge transfer process. At the meantime, the admittance (Y_0) of Z_W also increases gradually in stage Ⅱ, which corresponds to the decrease of diffusion resistance. It means that the diffusion process also becomes easy. Therefore, the corrosion of rebar is accelerated in stage Ⅱ.

The corrosion current density of the rebar can be calculated approximately according to the Stern-Geary equation:

$$I_{corr}=B/R_{ct}$$

where, I_{corr} represents the corrosion current density and B is the "Stern-Geary constant". A value of 52 mV and 26 mV is often used in the calculation of B for rebar in the passive and active states respectively [33, 34]. According to the criteria for estimating the corrosion extent of rebar, as shown in Table 2 [35], the rebar is in passive state when $I_{corr} < 0.1 \mu A \cdot cm^{-2}$. Therefore, the passive and active states can be distinguished by the value of I_{corr}. Figure 11 shows the evolution of I_{corr} with increasing dry/wet cycles. The change of I_{corr} corresponds to the corrosion evolution stages of the corrosion processes. It is verified by I_{corr} that the rebar is already in active state in stage Ⅰ (cycle 0), and the corrosion rate in stage Ⅰ is relative low. Then the corrosion rate increases quickly in stage Ⅱ (cycle 1~4) with increasing dry/wet cycles. A stable corrosion rate is reached in stage Ⅲ (cycle 5~14).

Table 2. Criteria for estimating rebar corrosion conditions

Corrosion Rate ($\mu A \cdot cm^{-2}$)	Extent of Corrosion
$I_{corr} < 0.1$	passive state
$0.1 < I_{corr} < 0.5$	low to moderate corrosion
$0.5 < I_{corr} < 1.0$	moderate to high corrosion
$I_{corr} > 1.0$	high corrosion

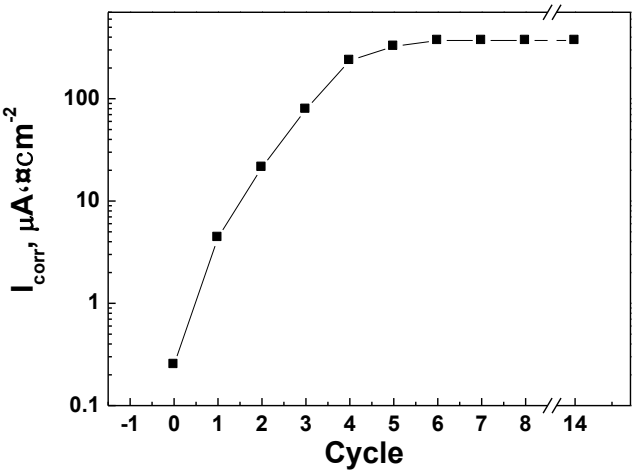

Figure 11. Evolution of I_{corr} with dry/wet cycles.

4. DISCUSSION

According to the above analysis, the corrosion of water-cooled rebar undergoes three stages with different characteristics. Comparing with the corrosion processes of bare rebar [13-15], the corrosion processes of scaled rebar are notably characterized by the active state during the curing period free of aggressive ions and the uniform corrosion type since the corrosion initiates.

For water-cooled rebar with oxide scale, the galvanic corrosion forms between the exposed rebar matrix at the defects in scale and the surrounding intact scale area during the curing period of stage Ⅰ, as discussed above. According to the E_{corr} result, the corrosion potential is -0.1 V (vs SHE) in the curing period. This potential is in the FeOOH stable region, as shown in the Pourbaix diagram of Fe-H_2O system (Figure 12) [36]. Therefore, at the exposed defects regions, the anode reactions that Fe transforms to FeOOH occur, as shown in equations (1) to (3). At the scale covered cathode regions, the oxygen reduction occurs, as shown in equation (4). Differing from the formation of a complete passive film on bare rebar, the γ-FeOOH only forms at the defect regions in the oxide scale, which can not protect the rebar from further corrosion. As there are a large number of defects in the scale, many small corrosion pits distributed uniformly in the steel surface, as shown in Figure 5. Eventually, the whole oxide scale is destroyed, and the uniform corrosion happens to the scaled rebar.

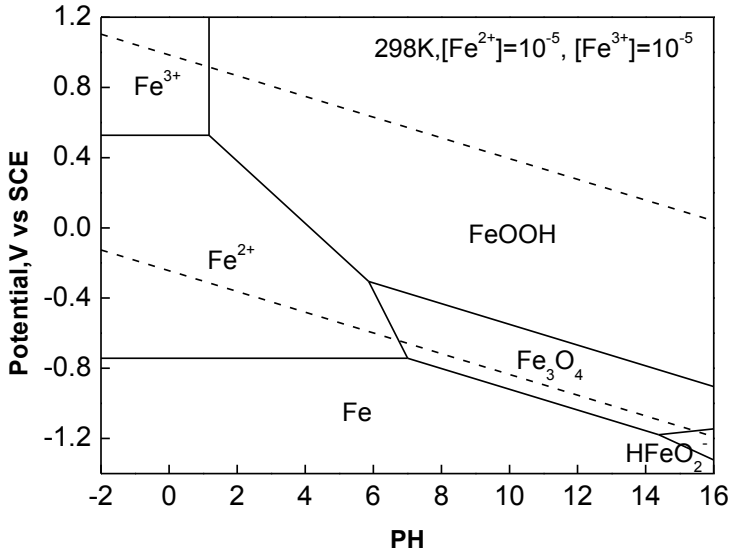

Figure 12. Pourbaix diagram of Fe-H_2O system

Anode reaction: $Fe \rightarrow Fe^{2+}+2e^-$ (1)

$Fe^{2+}+2OH^- \rightarrow Fe(OH)_2$ (2)

$Fe(OH)_2+OH^- \rightarrow \gamma\text{-}FeOOH+H_2O+e^-$ (3)

Cathode reaction: $H_2O+1/2O_2+2e^- \rightarrow 2OH^-$ (4)

In stage Ⅱ, when the corrosion product of γ-FeOOH exists on the rebar surface, the reduction of γ-FeOOH shown as equation (5) will happen prior to the reduction of oxygen at the cathode [37]. As this reaction can proceed without oxygen consumed, and it can consume Fe^{2+} and γ-FeOOH, the anode dissolution reactions will be promoted. Furthermore, when Cl^- exists in the concrete, it participates in the anodic reaction by generating intermediate product, as shown in equations (6) to (7) instead of equation (2). As the chloride ions are not consumed in the corrosion reactions, it can participate in the anodic depolarization reaction. This action will accelerate the corrosion process. Therefore, I_{corr} increases rapidly with the increase of the cycles.

Cathode reaction: $Fe^{2+}+8\gamma\text{-}FeOOH+2e^- \rightarrow 3Fe_3O_4+4H_2O$ (5)

Cl^- participating reaction: $Fe^{2+}+Cl^- \rightarrow [FeClcomplex]^+$ (6)

$[FeClcomplex]^++2OH^- \rightarrow Fe(OH)_2+Cl^-$ (7)

In stage Ⅲ, the rate controlling step of corrosion process is the diffusion process through a barrier layer. As the reduction of rust continues acting as cathode reaction, the corrosion rate can thus maintain a high value. Moreover, the γ-FeOOH and Fe_3O_4 will transform to more stable α-FeOOH if the duration is long enough. Therefore, the corrosion product consists of γ-FeOOH, Fe_3O_4 and α-FeOOH.

Among the three stages, the relative fast corrosion rate of stage Ⅱ and Ⅲ is both dominated by the diffusion process. Therefore, diffusion of reactants and products, including OH^-, Cl^- and Fe^{2+}, through the concrete and the rust layer is the dominate process influencing the corrosion of rebar. Control of diffusion by densification of the concrete and the rust layer or the initial oxide scale must be effective to slow down the corrosion.

5. CONCLUSIONS

The corrosion behavior of rebar can be described as uniform corrosion, and it evolved from slow rate corrosion stage, accelerated corrosion stage and constant rate corrosion stage. Furthermore, the rate determining step of electrode reactions changes from charge transfer to diffusion process with corrosion proceeds.

Comparing with the corrosion processes of bare rebar, the corrosion processes of scaled rebar are notably characterized by the active state during the curing period free of aggressive ions and the uniform corrosion type since the corrosion initiates.

During the long term corrosion process, the diffusion of reactants and products through the concrete and the rust layer is the dominate process influencing the corrosion rate of rebar.

References

1. O. Senhaji, R. Taouil, M. K. Skalli, M. Bouachrine, B. Hammouti, M. Hamidi, S.S. Al-Deyab, *Int. J. Electrochem. Sci.*, 6 (2011) 6300
2. U. Angst, B. Elsener, C.K. Larsen, Ø. Vennesland, *Cem. Concr. Res.*, 39 (2009) 11
3. C. A. Apostolopoulos, V. G. Papadakis, *Constr. Build. Mater.*, 22 (2008) 2316
4. Kazuaki Zen, *Corros. Sci.*, 47 (2005) 2353
5. W. Morris, V. M. Vazquez, *Corros. Rev.*, 20 (2002) 469
6. T. Cheewaket, Jaturapitakkul, W. Chalee, *Constr. Build. Mater.*, 37 (2012) 693
7. M. Nagayama and M. Cohen, *J Electrochem Soc.*, 109 (1962) 781
8. J. Kruger, JP. Calvert, *J Electrochem Soc.*, 114 (1967) 43
9. R. W. Revie, B. G. Baker and J. O'M Bockris, *J Electrochem Soc.*, 122 (1975) 1460
10. E O'G. William, *J Electrochem Soc.*, 127 (1980) 555
11. F. J. Martin, J. Olek, *Review of Scientific Instruments*, 74(2003) 2512
12. M. N. Haque, H. Al-Khaiat, *Cement Concrete Comp.*, 19 (1997) 123
13. Y. F. Cheng, J. L. Luo, *Electrochim. Acta*, 44 (1999) 2947
14. H. S. Wonga, Y. X. Zhao, A. R. Karimi, N. R. Buenfeld, W. L. Jin, *Corros. Sci.*, 52 (2010) 2469
15. R. J. Zhang, Arnaud Castel, Raoul François, *Cement Concrete Res.*, 39 (2009) 1077
16. Y. Z. Zhang, *Metallugical Stadardization & Quality*, 40 (2002) 37
17. D. L. Xing, J. Q. He, B. Wu, Q. M. Wan, *Corrosion & Protection*, 27(2006) 325

18. P. Ghods, O. B. Isgor, G. A. McRae, J. Li, G. P. Gu, *Corros. Sci.*, 53 (2011) 946
19. P. Ghods, O.B. Isgor, G. McRae, G.P. Gu, *Corros. Sci.*, 52 (2010) 1649
20. J. Wei, J. H Dong, E. H. Han, W. K., 24 (2010) 275
21. J. Wei, J. H Dong, W. K., *Corrosion Science and Protection Technology*, 21(2009), 468
22. J. Wei, J. H Dong, W. K., *Constr. Build. Mater.*, 25(2011) 1243
23. ASTM C876-91, Standard Test Method for Half-Cell Potentials of Uncoated Reinforcing Steel in Concrete[S].
24. C. Liu, Q. Bi, A. Leyland, A. Matthews, *Corros. Sci.*, 45 (2003) 1257
25. J. Q. Zhang, Ch. N. Cao, *Corrosion and protection*, 19(1998) 99
26. J. Flis, H. W. Pickering, K. Osseo-Asare, *Electrochimica Acta*, 43 (1998) 1921
27. C. Liu, Q. Bi, A. Leyland, A. Matthews, *Corros. Sci.*, 45 (2003) 1257
28. G. F. Qiao, J. P. Ou, *Electrochimica Acta*, 52 (2007) 8008
29. V. Feliu, J.A. Gonzalez, *Corros. Sci.*, 40 (1998) 975
30. V. Kolluru, Subramaniam, Mingdong Bi, *Corros. Sci.*, 51 (2009) 1976
31. A. Amirudin, D. Thierry, *Progress in Organic Coatings*, 26 (1995) 1
32. Cao Ch N, Zhang J Q, *Introduction of Electrochemical Impedance Spectra*, Science Press, Beijing, (2002)
33. C. Andrade and J. A. Gonzales, *Werkstoffe und Korrosion*, 29 (1978) 515
34. JA. González, C. Andrade, *British Corros J.*, 17(1982) 21
35. S. G. Millard, K. R. Gowers, Js. Gill, *American Concrete Institute SP 128*, Detroit, (1991) 373
36. M. Pourbaix, *Lectures on Electrochemical Corrosion*. Plenum Press, New York (1973)
37. I. Suzuki, N. Masuko, Y Hisamatsu, *Corros. Sci.*, 19 (1979) 521

© 2013 by ESG (www.electrochemsci.org)